

Self-assembled laminated nanoribbon-directed synthesis of noble metallic nanoparticle-decorated silica nanotubes and their catalytic applications†

Yiyang Lin, Yan Qiao, Yijie Wang, Yun Yan and Jianbin Huang*

Received 26th March 2012, Accepted 20th June 2012

DOI: 10.1039/c2jm31873c

Substrate-supported noble metallic nanoparticles have received intense attention owing to their great potential in various applications. In this work, silica nanotube-supported metallic nanoparticles (*i.e.*, Au, Ag, and Pd) are synthesized by *in situ* reducing metal ions into nanoparticles on the nanotube surface. The silica nanotubes are prepared through the traditional sol–gel approach using laminated nanoribbons as soft templates, which are self-assembled from dipeptide-amphiphiles. The surface of silica nanotubes is functionalized to display amino groups, which serve as active sites to host metallic particles. By changing the preparation conditions, the wall thickness of silica nanotubes is adjusted and the density of metallic nanoparticles on silica surface is facilely tuned. Finally the metallic nanoparticle-coated silica nanotubes are proven to be applicable in recyclable catalysis of 4-nitrophenol (4-NP) reduction.

Introduction

Nanostructured noble metallic particles are attracting tremendous attention owing to their versatile applications as catalysts and sensors and may prove important in optical, biological, and electronic devices.^{1–5} It has been realized that the metallic particles in the nanometer size regime show characteristic size-dependent properties (*e.g.*, electronic, optical, catalytic, and thermodynamic properties) different from bulk metals with significant size-effects occurring for 1–10 nm diameters. For example, the position of plasmon band from metallic NPs and its bandwidth is greatly influenced by the particle size.⁶ Also size effect is observed in surface-enhanced Raman scattering (SERS), where metallic nanoparticles are frequently exploited as substrates for signal enhancement.^{7,8} Therefore a facile route to synthesize nanosized metallic particles has become highly desirable.^{9–13}

On the other hand, the stability of metallic nanoparticles is another crucial issue for their further application. As the particle size is reduced, the surface energy of nanoparticles increases, making them unstable with high tendency for inter-particle aggregation. This will severely hinder the applications of metallic nanoparticles. For example, the aggregation of nanoparticles will greatly reduce their specific surface area and consequently lower

the catalytic efficiency. Due to the high cost and limited supply, however, the improvement of the catalytic efficiency and the reduction of the amounts used are the top priorities for practical applications. To solve these problems, organic molecules or polymers usually act as protective groups to prevent nanoparticles from coagulating by binding to the particle surface and enhance their stability. Frens pioneered the work of using sodium citrate to reduce chloroauric acid and stabilize the as-synthesized Au NPs.¹⁴ The other capping reagents include thiol-derivative containing hydrophilic groups,¹⁵ 4-(dimethylamino)pyridine,¹⁶ sodium cholate,¹⁷ *etc.* Alternatively, this problem can be solved by immobilizing metallic nanoparticles on supporting substrates such as silica dioxide (SiO₂), titanium dioxide (TiO₂), carbon nanotube (CNT), graphene, microgel, and polymer.^{18–45} This is regarded as a conventional way to stabilize metallic nanoparticles and particularly it combines the unique mechanical and electronic properties of nanotubes, wires, or fibers with the rich, size- and shape-dependent physicochemical properties of metallic nanoparticles. These hybrid nanomaterials have proven to have promising applications in catalysis, surface enhanced Raman spectroscopy (SERS), and sensors.^{22,35,46–48}

Inspired by these considerations, this work aims to synthesize silica nanotube (SNT)-supported noble metallic nanoparticles (*i.e.*, Au, Ag, and Pd) under ambitious conditions and explore their catalytic activity in the reaction of 4-nitrophenol reduction by sodium borohydride. The silica nanotubes are prepared *via* soft template-directed sol–gel method using tetraethylorthosilicate and 3-aminopropyltrimethoxysilane as precursor. Compared with the other strategies in synthesizing nanomaterials, soft template method exhibits remarkable advantages such as the rational controls on the size, shape, and composition.^{20,49–56} In this work, self-assembled laminated nanoribbons

Beijing National Laboratory for Molecular Sciences (BNLMS), State Key Laboratory for Structural Chemistry of Unstable and Stable Species, College of Chemistry, Peking University, Beijing 100871, People's Republic of China. E-mail: JBHuang@pku.edu.cn; Fax: +86-10-62751708; Tel: +86-10-62753557

† Electronic supplementary information (ESI) available: Time-dependent conversion of 4-NP catalyzed by Au-SNT, $\ln(C_t/C_0)$ profile *versus* reaction time. See DOI: 10.1039/c2jm31873c

from a dipeptide-amphiphile are exploited as the soft templates to rationally design silica nanotubes in a controllable manner. Particularly, amino groups are displayed on silica surface as active sites to *in situ* deposit metallic nanoparticles. Finally, the recyclable catalytic activities of SNT-supported metallic NPs are evaluated in the reaction of 4-nitrophenol reduction.

Materials and methods

Materials

The dipeptide-amphiphile C₄AzoGlyGly was synthesized according to our previous work.⁵⁷ Tetraethylorthosilicate (TEOS), 3-aminopropyltriethoxysilane (APS), and sodium tetrachloropalladate (Na₂PdCl₄) were bought from Sigma-Aldrich. Hydrochloroauric acid trihydrate (HAuCl₄·3H₂O, 99.9%), silver nitrate (AgNO₃) and the other reagents were obtained from Beijing Chemical Reagents Co. and used as received. Aqueous solutions were prepared using Milli-Q water of 18 MΩ.

Synthesis of silica nanotubes

The silica nanotubes were synthesized through a sol-gel process using self-assembled laminated nanoribbons as the soft template. First, laminated nanoribbons were obtained in the C₄AzoGlyGly/NaCl solution, which was prepared by adding C₄AzoGlyGly powder into sodium hydroxide solution and subsequently introducing desired amount of NaCl. The mixture was heated under stirring until the powder was completely dissolved. The sample was then slowly cooled to room temperature. Then, desired amounts of APS and TEOS were simultaneously introduced into C₄AzoGlyGly/NaCl solution followed by intense vortex on a vortex mixer. The mixture was kept at room temperature for 12 hours. Finally, the product was separated by centrifugation and purified by water/ethanol washing several times.

Synthesis of metallic nanoparticles on silica nanotubes

To prepare gold and silver nanoparticles-decorated silica nanotubes, the purified silica nanotubes were dispersed in 10 mM hydrochloroauric acid or silver nitrate solution. The mixture was kept at room temperature for 6 hours to reach equilibrium. The excess hydrochloroauric acid or silver nitrate was removed by centrifugation and water washing. After that, silica nanotubes were dispersed in water again and freshly prepared NaBH₄ solution was added to the suspension. After reaction for five hours, the products were isolated through centrifugation and purified by water washing to remove excess NaBH₄. To prepare palladium nanoparticles, silica nanotubes were rinsed in 10 mM hydrochloride solution for 10 min. After centrifugation and water washing, silica nanotubes were dispersed in 10 mM NaPdCl₄ solution at room temperature for 3 h. The unbound NaPdCl₄ was removed through centrifugation. After that, freshly prepared NaBH₄ was added to reduce Pd nanoparticles.

Characterization of self-assembled laminated nanoribbons

Self-assembled laminated nanoribbons were characterized using a JEM-100CXII transmission electron microscope (working

voltage of 80–100 kV) by the negative-staining method with uranyl acetate solution (1 wt%) as the staining agent. One drop of the C₄AzoGlyGly/NaCl solution was placed onto a carbon Formvar-coated copper grid (230 mesh) for 5 min. The excess liquid was sucked away by filter papers. Then one drop of the staining agent was placed onto the copper grid for 3 min. The excess staining agent was also sucked away by filter papers.

Characterization of silica nanotubes (SNT) and metallic nanoparticle-SNT composite

Silica nanotubes or metallic nanoparticles-decorated silica nanotubes were characterized by JEM-100CXII and JEM-2100. The inorganic nanotubes were initially dispersed in water and a drop of the dispersion was placed onto carbon Formvar-coated copper grid (230 mesh) dried in air. Energy dispersive spectrometer (EDS) results were obtained from Scanning Electron Microscope (SEM, Hitachi S4800). The UV-vis absorption spectra of the nanomaterial dispersions were collected on a Cary UV-vis spectrophotometer with incident light normal to the 1 cm path length quartz cuvette.

Evaluation of catalytic activity

The catalytic reduction reaction was carried out in a standard quartz cell with a 1 cm path length. The procedure entailed mixing excess NaBH₄ solution (2 mL, 50 mM) with a 4-NP solution (100 μL, 2 mM) in the quartz cell. After that 50 μL 0.40 mg mL⁻¹ silica nanotube-supported metallic nanoparticle suspension was added to the solution and the absorption spectra were recorded immediately by Cary UV-vis spectrophotometer with a time interval of 30 s at 25 °C.

Results and discussion

Supramolecular self-assembled laminated nanoribbons by a dipeptide-amphiphile

In our previous work,⁵⁷ a novel dipeptide-amphiphile C₄AzoGlyGly consisting of a hydrophobic part (*i.e.*, azobenzene and butyl group) and hydrophilic part (*i.e.*, glycyglycine) is synthesized (Fig. 1). Driven by the multiple weak intermolecular forces

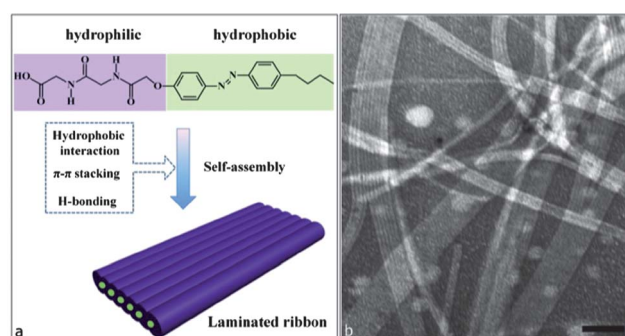


Fig. 1 (a) Molecular structure of a dipeptide-derived amphiphile C₄AzoGlyGly and the schematic illustration of supramolecular self-assembled laminated nanoribbons. (b) TEM image of laminated nanoribbons from C₄AzoGlyGly/NaCl (2 mM/20 mM). The sample is stained by 1.0 wt% uranyl acetate. The scale bar is 50 nm.

including hydrophobic interactions, hydrogen bond, and aromatic stacking, this molecule is found to self-assemble into laminated nanoribbons in water. In particular, self-assembled nanoribbons formation is promoted in the presence of sodium chloride. The nanoribbons are several micrometers long and tens of nanometers wide. As shown in Fig. 1b, the laminated nanoribbons are composed of well-aligned parallel nanofibers with obvious alternating bright and dark bands. The diameter of each fiber is calculated to be approximate 5 nm. These 1D ribbons further entangle with each other into 3D network, giving birth to robust elastic hydrogel. Owing to its responsiveness towards light and ionic strength, the hydrogel also shows its potential as a smart material.

Synthesis of silica nanotubes from laminated nanoribbons

It is expected that $C_4AzoGlyGly$ nanoribbons can be exploited as a soft template to synthesize 1D inorganic nanomaterials since the nanoribbons are stable and can be facilely prepared. In this work, tetraethoxysilane (TEOS) sol-gel polycondensation is conducted in $C_4AzoGlyGly/NaCl$ solution at room temperature. The silylating agent 3-aminopropyltrimethoxysilane (APS) is used as a catalyst. In a typical synthesis, 10 μL APS and 30 μL TEOS are added into 1.5 mL $C_4AzoGlyGly/NaCl$ solution (2 mM/20 mM) with intense vortexing. The mixture transforms into a rigid gel in a short time and is kept at room temperature for 12 h to complete the sol-gel reaction. As shown in the TEM image (Fig. 2), a large amount of silica nanotubes are obtained, in which the open ends of hollow nanotubes are clearly noted.

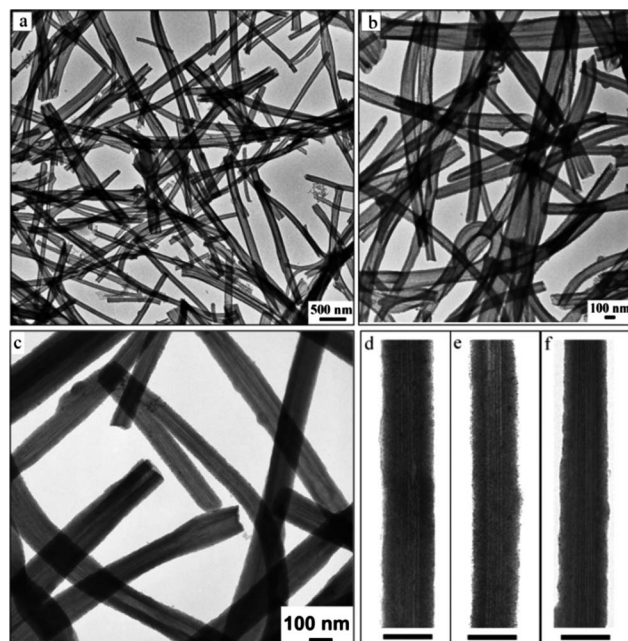


Fig. 2 Transmission electron microscopy (TEM) images: (a and b) silica nanotubes after completely removing the organic template by washing with ethanol and water; (c–f) silica nanotubes before removing the organic template. The enlarged TEM images in Fig. 2d–f show the laminated bands on silica nanotubes. The scale bars are 100 nm. The silica nanomaterials are synthesized in 1.5 mL $C_4AzoGlyGly/NaCl$ (2 mM/20 mM) with the addition of 10 μL APS and 30 μL TEOS.

The enlarged TEM image in Fig. 2b indicates the wall thickness of silica nanotubes is 20–30 nm.

To verify the templating effect of $C_4AzoGlyGly/NaCl$ nanoribbons, the as-synthesized silica nanotubes without template removal are characterized by TEM. As shown in Fig. 2c and d, laminated bands with well-aligned alternating dark stripes and bright stripes can be observed on silica nanotubes. The total width of these bands is 50–60 nm, while the width of each stripe is calculated to be 5–6 nm. This is in well agreement with the structural characteristics of $C_4AzoGlyGly$ laminated ribbons (Fig. 1b). It is believed that these bands are ascribed to the laminated ribbons consisting of parallel nanofibers inside silica nanotubes. We therefore confirm the existence of laminated nanoribbons encapsulated inside the as-synthesized silica nanotubes and their role as a soft template in the sol-gel transcription.

The influence of TEOS and APS concentration on the morphology of silica nanotubes is investigated. Herein, the concentration of $C_4AzoGlyGly/NaCl$ solution is kept at 2 mM/20 mM and the volume is 1.5 mL. When the amount of TEOS and APS is relatively small (APS/TEOS = 4 $\mu\text{L}/12 \mu\text{L}$), the as-prepared silica nanotubes look like thin sheets with the wall thickness of ~ 5 nm (Fig. 3a). When the amount of precursor APS/TEOS is 14 $\mu\text{L}/42 \mu\text{L}$ and 20 $\mu\text{L}/60 \mu\text{L}$, the wall thickness of silica nanotubes increases to 30 nm and 45 nm respectively (Fig. 3b and c). The nanotube wall thickness further grows to ~ 60 nm with the addition of 40 μL APS and 120 μL TEOS (Fig. 3d). It is therefore demonstrated that the wall thickness of silica nanotubes can be effectively tuned by simply adjusting the amount of silica precursor APS/TEOS.

It seems that APS is indispensable as a catalyst in template-directed sol-gel transcription in this work. To further evaluate the role of APS in this process, two control experiments are

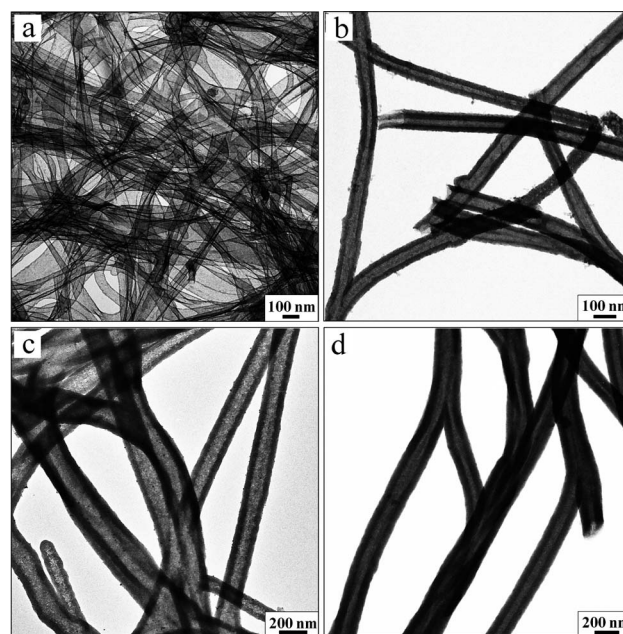


Fig. 3 Morphological variation of silica nanotubes synthesized in 1.5 mL $C_4AzoGlyGly/NaCl$ mixture (2 mM/20 mM) with different APS/TEOS volume ratios. (a) 4 $\mu\text{L}/12 \mu\text{L}$; (b) 14 $\mu\text{L}/42 \mu\text{L}$; (c) 20 $\mu\text{L}/60 \mu\text{L}$; (d) 40 $\mu\text{L}/120 \mu\text{L}$.

performed. First, the TEOS hydrolyzation reaction is studied in $C_4AzoGlyGly/NaCl/TEOS$ mixture in the absence of APS, in which TEOS hydrolysis is not detected. This result suggests the importance of catalyst in this reaction. In the second experiment, ammonia solution is introduced into $C_4AzoGlyGly/NaCl/TEOS$ mixture as a catalytic reagent. According to the literature, TEOS will be hydrolyzed into the intermediate species (*i.e.*, oligomeric siloxanes) in the presence of ammonia.^{53,58} However, no silica nanotubes are observed under TEM, implying the special role of APS in this experiment. It is speculated that anionic oligomeric siloxanes cannot adsorb onto the negative $C_4AzoGlyGly$ nanoribbons due to electrostatic repulsion and consequently silica nanotubes are not obtained. Hence APS is supposed to play dual functions in the process of silica nanotubes formation. On one hand, the amino group on APS serves as a basic catalyst to trigger TEOS hydrolysis into oligomeric siloxanes in water. On the other hand, the positive charge on the amino group enables APS as well as its hydrolyzed product to adsorb onto negative $C_4AzoGlyGly$ nanoribbons through electrostatic attraction, forming layers of hydroxyl groups (Si–OH) on nanoribbons surface. This will reduce the negative charge on the template and greatly facilitate the adsorption of oligomeric siloxanes onto nanoribbons. As a result, sol–gel transcription from nanoribbons into silica nanotubes are realized. In addition, the introduction of APS also functionalizes silica nanotubes with amino groups on the surface.

In situ synthesis of metallic nanoparticles on silica nanotubes

Since the silica nanotubes are functionalized with amino groups by APS, they are expected to serve as substrates for reducing noble metallic nanoparticles.^{22,26} In this work, the amino-modified silica nanotubes are exploited to *in situ* synthesize gold nanoparticles, in which amino groups are the active sites. In detail, silica nanotubes are rinsed in $HAuCl_4$ solution to allow complete adsorption of $HAuCl_4$ on amino groups. After removing the unbound $HAuCl_4$ by centrifugation, the nanotubes are further dispersed in water followed by the addition of fresh $NaBH_4$. As shown in Fig. 4a and b, silica nanotube-supported gold nanoparticles (Au-SNT) with the mean Au NPs diameter of 5 nm are observed in TEM. The formation of gold nanoparticles is also confirmed by surface plasmon resonance (SPR). The UV-vis spectrum of the as-prepared Au-SNT suspension shows a typical absorption profile with a well-resolved peak located at 540 nm (Fig. 4c). The change of sample appearance from white to a wine-red color is also supportive of Au NPs formation (inset in Fig. 4c). The energy-dispersive X-ray spectrum (EDS) confirmed the existence of gold on silica nanotubes.

Owing to the expecting coordination between silver ions (Ag^+) and amino groups ($-NH_2$), the amino-modified silica nanotubes are utilized as a scaffold to reduce silver nanoparticles by $NaBH_4$. As shown in Fig. 5a and b, an abundance of Ag nanoparticles with the diameters ranging from 3 nm to 8 nm on the SNT surface can be seen in TEM images. The reduction of silver ions is accompanied by the appearance of yellow color in silica nanotubes suspension, which is caused by Ag nanoparticle surface plasmon resonance. This can be manifested from the UV-vis spectrum in Fig. 5c, in which Ag NPs plasmon peak is located at 416 nm. Although it is difficult to quantify the Ag particles

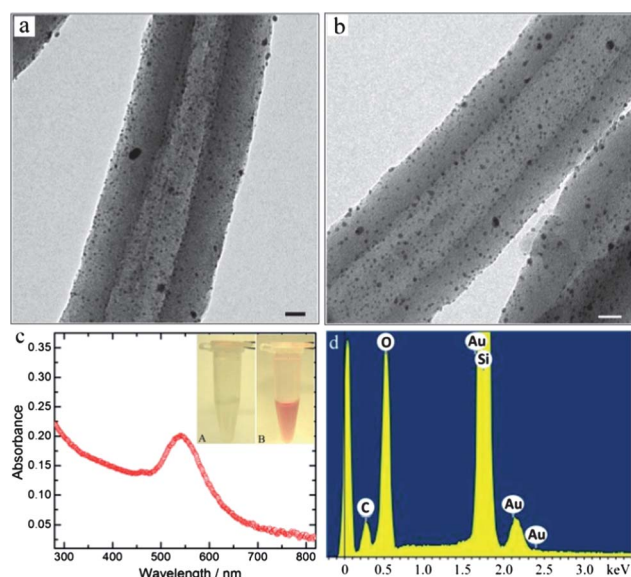


Fig. 4 (a–b) High-resolution TEM images of silica nanoparticles coated with gold nanoparticles (scale bar: 20 nm); (c) UV-vis spectrum of Au-SNT suspension. The insets are the macroscopic photos of (A) $HAuCl_4/SNT$ suspension and (B) Au-SNT suspension; (d) EDS spectrum of Au-SNT nanocomposite. The silica nanotubes are prepared from 1.5 mL $C_4AzoGlyGly/NaCl$ (2 mM/20 mM) solution with APS/TEOS = 10 μ L/30 μ L.

density on SNT, the coverage of Ag nanoparticles on silica nanotubes is significantly higher than that of Au-SNT nanocomposite. This is because strong silver/amino coordination enables better adsorption of silver ions on silica surface, leading

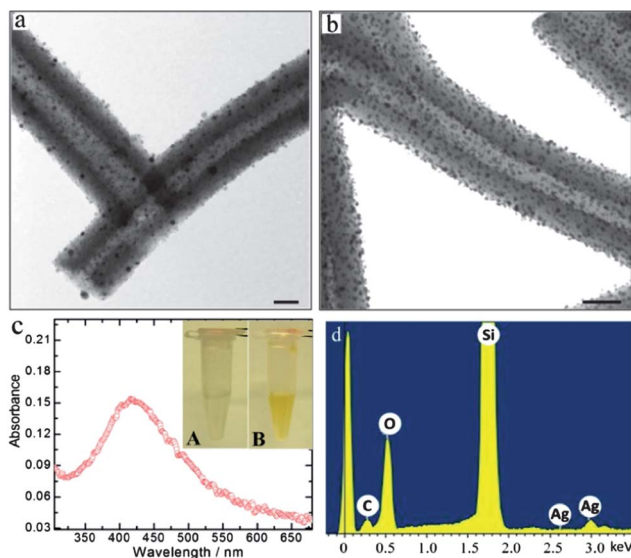


Fig. 5 (a–b) TEM images of silver nanoparticles-loaded silica nanotubes (Ag-SNT). The scale bar is 50 nm. (c) UV-vis spectrum of Ag-SNT suspension. The inset shows the macroscopic picture of (A) silica nanotube/ $AgNO_3$ suspension and (B) Ag-SNT suspension in water; (d) EDS spectrum of Ag-SNT composite. The silica nanotubes are prepared from 1.5 mL $C_4AzoGlyGly/NaCl$ (2 mM/20 mM) solution with APS/TEOS = 10 μ L/30 μ L.

to higher loading effectiveness of Ag NPs. The result of EDS analysis is presented in Fig. 5d, in which the intense peak at around 3 keV supports Ag NPs existence.

In addition, the amino-functionalized silica nanotubes are exploited to synthesize palladium nanoparticles. However, the synthetic process is different from the protocol of Au or Ag nanoparticles. In this work, silica nanotubes are treated with hydrochloride solution (\sim pH 2) to allow completely protonation of amino groups. The acid-treated silica nanotubes are rinsed in NaPdCl_4 solution for 3 h at room temperature. It is believed that protonated silica nanotubes will adsorb anionic PdCl_4^{2-} benefiting from electrostatic attraction. Subsequently, the precursor PdCl_4^{2-} is reduced into Pd^0 with the addition of NaBH_4 , giving rise to a clear-brown suspension (Fig. 6a and b). The TEM image clearly shows that Pd nanoparticles deposited on silica nanotubes (Pd-SNT) are almost-monodisperse and their shape is roughly spherical (Fig. 6c). Unbounded Pd NPs are hardly observed. The purity of Pd-SNT nanocomposites is verified by energy-dispersive X-ray analysis (EDS, Fig. 6d).

Catalytic activity

The catalytic activity of silica nanotubes-supported metallic nanoparticles is tested by the reduction of 4-nitrophenolate (4-NP) to 4-aminophenolate (4-AP) in the presence of NaBH_4 . It is well-known that 4-nitrophenol solution exhibits a strong absorption peak at 317 nm which is remarkably red-shifted to 400 nm when treated with an aqueous solution of NaBH_4 .^{23–25,37,40,41,59} The absorption at 400 nm comes from the formation of 4-nitrophenolate ions owing to an increase in solution alkalinity upon the addition of NaBH_4 . In the absence of metallic nanoparticles, the peak at 400 nm stays unchanged. However, this peak starts to decrease with reaction time in the presence of Au-SNT, suggesting the reduction of 4-NP (Fig. 7a).

The catalytic activities of the heterostructures with different nanoparticles (*i.e.*, Au, Pd, and Ag) on silica nanotubes are

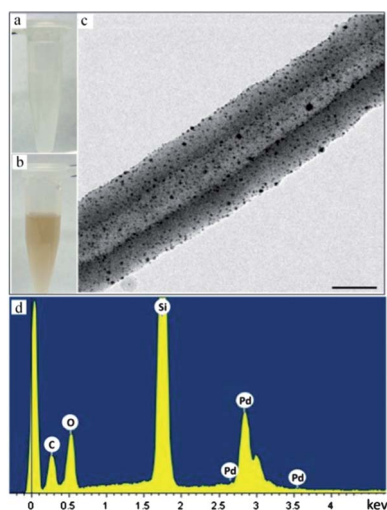


Fig. 6 Macroscopic appearance of the suspension: (a) Na_2PdCl_4 -SNT and (b) Pd-SNT. (c) TEM image and (d) EDS spectrum of palladium-decorated silica nanotubes (Pd-SNT). The scale bar is 50 nm. The silica nanotubes are prepared from 1.5 mL $\text{C}_4\text{AzoGlyGly/NaCl}$ (2 mM/20 mM) solution with $\text{APS/TEOS} = 10 \mu\text{L}/30 \mu\text{L}$.

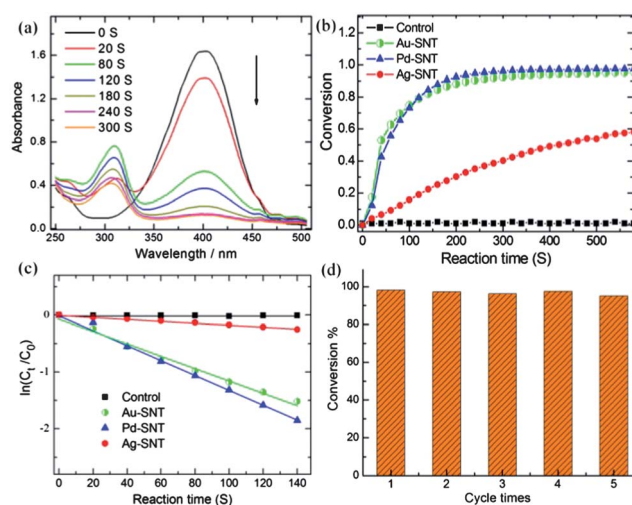


Fig. 7 (a) Time-dependent UV-vis absorbance of 4-NP catalyzed by silica nanotube-supported gold nanoparticles (Au-SNT). (b) Time-dependent conversion of 4-NP reduction catalyzed by Au-SNT, Ag-SNT, and Pd-SNT. (c) $\ln(C_t/C_0)$ versus reaction time. (d) Catalytic conversion of 4-NP by using recycled Au-SNT at different cycle times. The silica nanotubes are prepared from 1.5 mL $\text{C}_4\text{AzoGlyGly/NaCl}$ (2 mM/20 mM) solution with $\text{APS/TEOS} = 10 \mu\text{L}/30 \mu\text{L}$.

compared in the reaction of 4-NP reduction. The reaction conversion is calculated from C_t/C_0 , which is measured from the relative intensity of UV-vis absorbance (A_t/A_0) at 400 nm. Herein, C_t is the concentration of 4-NP at the reaction time t and C_0 is the initial concentration. As Fig. 7b shows, the reaction is hardly noticeable in the absence of metallic nanoparticles. In the presence of Au-SNT and Pd-SNT, the reaction proceeds rapidly with the conversion exceeding 90% at a reaction time of 200 s. However, the catalytic activity of Ag-SNT is significantly lower and the conversion is lower than 60% even when the reaction time reaches 600 s. In our experiment, the concentration of NaBH_4 is significantly higher than that of 4-NP and can be considered as constant during the reaction period. So the pseudo first-order kinetics can be applied to evaluate the reaction rate constants. As shown in Fig. 7c, the linear relationship of $\ln(C_t/C_0)$ versus reaction time (t) indicates that the reduction of 4-NP by these heterostructures follows the pseudo first-order kinetics. The reaction rate constants are calculated to be $k_{\text{Pd-SNT}} \sim 0.0131 \text{ s}^{-1}$, $k_{\text{Au-SNT}} \sim 0.0116 \text{ s}^{-1}$, and $k_{\text{Ag-SNT}} \sim 0.00175 \text{ s}^{-1}$. The rate constants are comparable to^{24,60,61} or higher than^{25,36,62,63} that of substrate-supported metallic nanoparticles in the literature. It is realized that the rate of electron transfer (from BH_4^- ion to 4-nitrophenol) at the metal surface can be influenced by the diffusion rate of 4-nitrophenol to the metal surfaces, diffusion rate of 4-aminophenol away from the surface, and the interfacial electron transfer rate.⁴² When heterogeneous charge transfer is faster than diffusion, the diffusion rate of 4-nitrophenol and 4-aminophenol plays an important role. Compared to dendrimer or microgel protected metallic NPs, or silica coated NPs, the Au NPs on Au-SNTs in this work are largely exposed to water without coating polymers or silica shells, and hence the reactant diffusion to metallic surface and product diffusion away from particle surface is not hindered. In addition, the large exposed particle surface of our Au-SNTs may also contribute to

the relatively high reaction rate. Specifically, the catalytic activity is compared with that of silica nanotubes immobilized Au NPs in the literature. Shao reports Au NPs assembled on electrospun silica nanotubes with the reduction rate constant of $10.64 \times 10^{-3} \text{ s}^{-1}$.⁶¹ Jan uses layer-by-layer polypeptide assemblies to mediate the synthesis of Au/mesoporous SNTs with the apparent rate constant of 3×10^{-4} and $8 \times 10^{-4} \text{ s}^{-1}$ for Au/SNTs obtained from (Lys₃₄₀/Glu₁₂₅)₅ and (Lys₃₄₀/PLT)₅ coated membranes.⁶⁴ It is therefore proposed that our Au-SNTs nanocomposite shows good catalytic activity for 4-NP reduction. In addition, the catalytic efficiency of the nanocomposites with different metallic NPs coverage is studied. It seems that the Au NPs coverage on silica surface does not significantly affect the reaction rate although high Au NPs coverage yields slightly high reaction rate constant (Fig. S1†).

The reusability of the Au-SNT nanocomposite as a catalyst is also investigated. As shown in Fig. 7d, the Au-SNT catalyst could be recycled five times without any significant loss of reaction conversion. In the fifth run, the conversion yield of 4-NP is still as high as 95% after the reaction time of 2000 s. The high conversion after five cycles is probably ascribed to good dispersion of gold nanoparticles on silica nanotubes and their high stability.

Conclusions

This work presents a cost-effective experiment to design silica nanotubes (SNT) with tunable wall thickness through a sol-gel method by using self-assembled laminated nanoribbons as a soft template. The surface of silica nanotubes is functionalized to display amino groups, which serve as active sites to deposit metallic nanoparticles (*i.e.*, Au, Ag, and Pd) under ambitious conditions. The metallic nanoparticle-SNT composites are employed in recyclable catalysis of 4-nitrophenol reduction by NaBH₄. Considering the fact that amino groups can host a series of metal ions (*e.g.*, Ni²⁺, Cu²⁺, and Pt²⁺), our silica nanotubes are anticipated to be exploited as a platform to synthesize more metallic nanoparticles, such as Ni, Cu and Pt. We hope this work can shed a light on the versatile applications of supramolecular nanostructures in nanochemistry and provide new recyclable catalysts for heterogeneous catalysis.

Acknowledgements

This work is supported by National Natural Science Foundation of China (51121091 and 21073006) and Doctoral Program of Higher Education of China.

Notes and references

- M. C. Daniel and D. Astruc, *Chem. Rev.*, 2004, **104**, 293–346.
- A. Chen and P. Holt-Hindle, *Chem. Rev.*, 2010, **110**, 3767–3804.
- M. R. Jones, K. D. Osberg, R. J. Macfarlane, M. R. Langille and C. A. Mirkin, *Chem. Rev.*, 2011, **111**, 3736–3827.
- P. Ghosh, G. Han, M. De, C. K. Kim and V. M. Rotello, *Adv. Drug Delivery Rev.*, 2008, **60**, 1307–1315.
- C. J. Murphy, A. M. Gole, J. W. Stone, P. N. Sisco, A. M. Alkilany, E. C. Goldsmith and S. C. Baxter, *Acc. Chem. Res.*, 2008, **41**, 1721–1730.
- S. Link and M. A. El-Sayed, *J. Phys. Chem. B*, 1999, **103**, 4212–4217.
- S. M. Nie and S. R. Emery, *Science*, 1997, **275**, 1102–1106.
- J. T. Krug, G. D. Wang, S. R. Emory and S. M. Nie, *J. Am. Chem. Soc.*, 1999, **121**, 9208–9214.
- N. R. Jana and X. G. Peng, *J. Am. Chem. Soc.*, 2003, **125**, 14280–14281.
- N. R. Jana, L. Gearheart and C. J. Murphy, *Chem. Mater.*, 2001, **13**, 2313–2322.
- N. R. Jana, L. Gearheart and C. J. Murphy, *Langmuir*, 2001, **17**, 6782–6786.
- K. R. Brown and M. J. Natan, *Langmuir*, 1998, **14**, 726–728.
- L. O. Brown and J. E. Hutchison, *J. Am. Chem. Soc.*, 1997, **119**, 12384–12385.
- G. Frens, *Nature, Phys. Sci.*, 1973, **241**, 20–22.
- W. P. Wuelfling, S. M. Gross, D. T. Miles and R. W. Murray, *J. Am. Chem. Soc.*, 1998, **120**, 12696–12697.
- D. I. Gittins and F. Caruso, *Angew. Chem., Int. Ed.*, 2001, **40**, 3001–3004.
- Y. Qiao, H. Chen, Y. Lin and J. Huang, *Langmuir*, 2011, **27**, 11090–11097.
- S. Zhang, W. Ni, X. Kou, M. H. Yeung, L. Sun, J. Wang and C. Yan, *Adv. Funct. Mater.*, 2007, **17**, 3258–3266.
- S. Liu and M.-Y. Han, *Chem.–Asian J.*, 2010, **5**, 36–45.
- D. R. Bae, S. J. Lee, S. W. Han, J. M. Lim, D. Kang and J. H. Jung, *Chem. Mater.*, 2008, **20**, 3809–3813.
- J. Lee, J. C. Park and H. Song, *Adv. Mater.*, 2008, **20**, 1523–1528.
- V. V. R. Sai, D. Gangadean, I. Niraula, J. M. F. Jabal, G. Corti, D. N. McIlroy, D. E. Aston, J. R. Branen and P. J. Hrdlicka, *J. Phys. Chem. C*, 2011, **115**, 453–459.
- J. P. Ge, Q. Zhang, T. R. Zhang and Y. D. Yin, *Angew. Chem., Int. Ed.*, 2008, **47**, 8924–8928.
- G. Tong, T. Liu, S. Zhu, B. Zhu, D. Yan, X. Zhu and L. Zhao, *J. Mater. Chem.*, 2011, **21**, 12369–12374.
- S.-H. Wu, C.-T. Tseng, Y.-S. Lin, C.-H. Lin, Y. Hung and C.-Y. Mou, *J. Mater. Chem.*, 2011, **21**, 789–794.
- X. Du and J. He, *Nanoscale*, 2012, **4**, 852–859.
- H. Tada, T. Kiyonaga and S.-i. Naya, *Chem. Soc. Rev.*, 2009, **38**, 1849–1858.
- B. Xue, P. Chen, Q. Hong, J. Y. Lin and K. L. Tan, *J. Mater. Chem.*, 2001, **11**, 2378–2381.
- S. Hrapovic, E. Majid, Y. Liu, K. Male and J. H. T. Luong, *Anal. Chem.*, 2006, **78**, 5504–5512.
- B. Yoon, H.-B. Pan and C. M. Wai, *J. Phys. Chem. C*, 2009, **113**, 1520–1525.
- J. John, E. Gravel, A. Hagege, H. Li, T. Gacoin and E. Doris, *Angew. Chem., Int. Ed.*, 2011, **50**, 7533–7536.
- M. A. Correa-Duarte and L. M. Liz-Marzan, *J. Mater. Chem.*, 2006, **16**, 22–25.
- J. Guerra and M. Antonia Herrero, *Nanoscale*, 2010, **2**, 1390–1400.
- X. Huang, X. Qi, F. Boey and H. Zhang, *Chem. Soc. Rev.*, 2012, **41**, 666–686.
- S. Wunder, F. Polzer, Y. Lu, Y. Mei and M. Ballauff, *J. Phys. Chem. C*, 2010, **114**, 8814–8820.
- Y. Mei, Y. Lu, F. Polzer, M. Ballauff and M. Drechsler, *Chem. Mater.*, 2007, **19**, 1062–1069.
- Y. Lu, Y. Mei, M. Drechsler and M. Ballauff, *Angew. Chem., Int. Ed.*, 2006, **45**, 813–816.
- Y. H. He, J. Y. Yuan and G. Q. Shi, *J. Mater. Chem.*, 2005, **15**, 859–862.
- D. Astruc, F. Lu and J. R. Aranzaes, *Angew. Chem., Int. Ed.*, 2005, **44**, 7852–7872.
- K. Hayakawa, T. Yoshimura and K. Esumi, *Langmuir*, 2003, **19**, 5517–5521.
- T. Endo, T. Yoshimura and K. Esumi, *J. Colloid Interface Sci.*, 2005, **286**, 602–609.
- K. Esumi, R. Isono and T. Yoshimura, *Langmuir*, 2004, **20**, 237–243.
- R. Contreras-Caceres, A. Sanchez-Iglesias, M. Karg, I. Pastoriza-Santos, J. Perez-Juste, J. Pacifico, T. Hellweg, A. Fernandez-Barbero and L. M. Liz-Marzan, *Adv. Mater.*, 2008, **20**, 1666–1670.
- M. Karg and T. Hellweg, *J. Mater. Chem.*, 2009, **19**, 8714–8727.
- M. Das, L. Mordoukhovski and E. Kumacheva, *Adv. Mater.*, 2008, **20**, 2371–2375.
- Z. Wu, Y. Lv, Y. Xia, P. A. Webley and D. Zhao, *J. Am. Chem. Soc.*, 2012, **134**, 2236–2245.
- Z. Yin, Q. He, X. Huang, J. Zhang, S. Wu, P. Chen, G. Lu, Q. Zhang, Q. Yan and H. Zhang, *Nanoscale*, 2012, **4**, 293–297.

- 48 P. Sharma, S. C. Brown, A. Singh, N. Iwakuma, G. Pyrgiotakis, V. Krishna, J. A. Knapik, K. Barr, B. M. Moudgil and S. R. Grobmyer, *J. Mater. Chem.*, 2010, **20**, 5182–5185.
- 49 M. Llusar and C. Sanchez, *Chem. Mater.*, 2008, **20**, 782–820.
- 50 Y. Y. Lin, Y. Qiao, C. Gao, P. F. Tang, Y. Liu, Z. B. Li, Y. Yan and J. B. Huang, *Chem. Mater.*, 2010, **22**, 6711–6717.
- 51 Y. Qiao, Y. Wang, Z. Yang, Y. Lin and J. Huang, *Chem. Mater.*, 2011, **23**, 1182–1187.
- 52 X. J. Wu, S. J. Ji, Y. Li, B. Z. Li, X. L. Zhu, K. Hanabusa and Y. G. Yang, *J. Am. Chem. Soc.*, 2009, **131**, 5986–5993.
- 53 J. H. Jung, H. Kobayashi, M. Masuda, T. Shimizu and S. Shinkai, *J. Am. Chem. Soc.*, 2001, **123**, 8785–8789.
- 54 K. J. C. van Bommel, A. Friggeri and S. Shinkai, *Angew. Chem., Int. Ed.*, 2003, **42**, 980–999.
- 55 S. Mann, *Nat. Mater.*, 2009, **8**, 781–792.
- 56 Y. Qiao, Y. Y. Lin, Y. J. Wang, Z. Y. Yang, J. Liu, J. Zhou, Y. Yan and J. B. Huang, *Nano Lett.*, 2009, **9**, 4500–4504.
- 57 Y. Lin, Y. Qiao, P. Tang, Z. Li and J. Huang, *Soft Matter*, 2011, **7**, 2762–2769.
- 58 C. J. Brinker, *J. Non-Cryst. Solids*, 1988, **100**, 31–50.
- 59 S. Sarkar, A. K. Sinha, M. Pradhan, M. Basu, Y. Negishi and T. Pal, *J. Phys. Chem. C*, 2011, **115**, 1659–1673.
- 60 F.-H. Lin and R.-A. Doong, *J. Phys. Chem. C*, 2011, **115**, 6591–6598.
- 61 Z. Zhang, C. Shao, P. Zou, P. Zhang, M. Zhang, J. Mu, Z. Guo, X. Li, C. Wang and Y. Liu, *Chem. Commun.*, 2011, **47**, 3906–3908.
- 62 R. Wang, X. Jiang, B. Yu and J. Yin, *Soft Matter*, 2011, **7**, 8619–8627.
- 63 L. Lin, K. Shang, X. Xu, C. Chu, H. Ma, Y.-I. Lee, J. Hao and H.-G. Liu, *J. Phys. Chem. A*, 2011, **115**, 11113–11118.
- 64 J.-S. Jan, T.-H. Chuang, P.-J. Chen and H. Teng, *Langmuir*, 2011, **27**, 2834–2843.